

Automated derivation of urban building density information using airborne LiDAR data and object-based method

Bailang Yu^{a,*}, Hongxing Liu^b, Jianping Wu^a, Yingjie Hu^a, Li Zhang^a

^a Key Laboratory of Geographic Information Science, Ministry of Education, East China Normal University, 3663 North Zhongshan Rd., Shanghai 200062, PR China

^b Department of Geography, University of Cincinnati, Cincinnati, OH 45221, USA

ARTICLE INFO

Article history:

Received 18 February 2010
Received in revised form 21 June 2010
Accepted 15 August 2010
Available online 15 September 2010

Keywords:

Building density
Building Coverage Ratio
Floor Area Ratio
Object-based method
LiDAR

ABSTRACT

Building density information is fundamentally important for urban design, planning and management and for urban environmental studies. This paper demonstrates that Building Coverage Ratio (BCR), Floor Area Ratio (FAR), and other building density indicators can be numerically and automatically derived from high-resolution airborne LiDAR data. An object-based method is proposed to process the LiDAR data for the building density information. The method consists of a sequence of numerical operations: generating the normalized Digital Surface Model (nDSM), extracting building objects, deriving object attributes, associating objects with the corresponding land lots, and computing building density indicators at land lot and urban district scales. The algorithms for these operations have been implemented as an ArcGIS extension module. The object-based method is applied to the processing of airborne LiDAR data over downtown Houston. Various attributes have been derived to quantify the building density, urban physical structure, and landscape morphological characteristics of the downtown area at three different spatial scales.

© 2010 Elsevier B.V. All rights reserved.

1. Introduction

In recent decades, numerous metropolitan areas around the world have experienced continued horizontal expansions and sprawls through the decentralization process, while many cities have also shown a land use intensification trend (Narayan, 1996). The intensification trend is indicated by denser and taller buildings through various urban renewal and redevelopment projects of inner cities (Greer, 1980; Narayan, 1996; Weiss, 1992). As a natural response to dense business concentration and land scarcity, an increasing number of high-rise buildings and skyscrapers have settled in downtowns of many large metropolitan areas (Frenkel, 2007; Hartshorn, 1992; Weiss, 1992), which define the skyline and reshape scenic sight and aesthetical beauty of the cities.

Many modern cities in Asia have already adopted the vertical development strategy not only for their downtowns and central business districts (CBDs) but also for residential districts to tackle urban land scarcity problems. High-rise residential clusters and strips have emerged in Hong Kong, Tokyo, Singapore, Shanghai, Beijing, Taipei, Kuala Lumpur, Soul, and other cities (Chau et al., 2007; Wang and Chien, 1999; Wong, 2004). The buildings of varying heights increase the morphological heterogeneity and vertical

roughness of urban space, influence wind flow (Cionco and Ellefsen, 1998) and sunlight distribution (Oke, 1988; Robinson, 2006; Swaid, 1993), and mold the urban microclimate (Adolphe, 2001). Several studies reported that the building density affects the wind conditions at pedestrian level (Kubota et al., 2008), the access of sunlight and solar radiation (Lam, 2000; Miguet and Groleau, 2002; Oke, 1988; Robinson, 2006; Swaid, 1993; Yu et al., 2009a), the interior temperatures of buildings (Mills, 1997), the surface thermal conditions (Streutker, 2003), the dispersion of atmospheric pollutants (Theodoridis and Moussiopoulos, 2000), and land subsidence (Cui et al., 2010). The information on the morphology and density of the buildings is essential for empirical and scientific investigation of these urban environmental and social issues.

To ameliorate adverse urban environmental and social problems, the building density regulations such as lot size zoning, building height, and/or Floor Area Ratio (FAR) restrictions are common practices in urban planning and management in many countries over the world (Arnott and MacKinnon, 1977; Bertaud and Brueckner, 2005). Examples include USA (Weiss, 1992), Japan (Gao et al., 2006; Joshi and Kono, 2009; Kono et al., 2008; Kubota et al., 2008), India (Bertaud and Brueckner, 2005; Narayan, 1996), China (Chau et al., 2007; Cui et al., 2010; Liao et al., 2007; Pan et al., 2008), and Singapore (Wong, 2004). Many cities have imposed building height limits beginning in the late nineteenth century, when the skyscraper first emerged as a new urban form. Chicago and New York were the first cities to place a flat limitation on build-

* Corresponding author. Tel.: +86 21 62232946; fax: +86 21 62232946.
E-mail address: blyu@geo.ecnu.edu.cn (B. Yu).

ing heights (Weiss, 1992). By the early 1900s, a few cities, such as Boston and Washington, DC, introduced differential height limitations by districts rather than imposing one limit on the entire city. Based on aesthetic considerations, building height restrictions are often imposed for historical and scenic districts of many cities, such as Washington, DC, Canberra, Paris, and Beijing. Lot size zoning is imposed to directly control the size of each lot containing one household. The FAR regulation is imposed in the urban area to limit the building's volume of floor space while permitting more flexibility in the shape of the structure. Lot size regulation and FAR regulations are both intended to control building density to minimize the adverse environmental problems. Maximum FAR regulations indirectly control the size and height of buildings and affect the building density and urban spatial structure. Sometimes, minimum FAR regulation may be also enforced to increase building density or to prevent underdevelopment (Joshi and Kono, 2009). Regulations with relatively low maximum height and FAR restrictions encourage low-density horizontal expansion, resulting more dispersed pattern of urbanization. Urban population growth rate and hence the level of adverse environment effects in a city can change remarkably over time. Therefore, building density regulation was also changed concomitantly with different urban development stages (Weiss, 1992).

Urban districts constructed in different time periods show significant difference in building density and structures. With the improvements of technologies in construction, air conditioning, heating and ventilation, the maximum permitted building heights have been raised in many cities (Chau et al., 2007; Pan et al., 2008; Weiss, 1992), promoting urban vertical growth and land use intensification. Many newly developed commercial and residential districts have higher FAR and lower Building Coverage Ratio (BCR), compared with old ones (Pan et al., 2008). Timely and complete information about urban building density and morphology is required for the assessment of land use intensity and efficiency, design and adjustment of zoning regulations and land use policy, monitoring and enforcement of urban management policies (Fu and Somerville, 2001; Gao et al., 2006; Kubota et al., 2008; Liao et al., 2007; Pan et al., 2008; Theodoridis and Moussiopoulos, 2000).

In reality, quantitative information about urban buildings is often unavailable, incomplete, or out-of-date. Although original building plans contain detailed information, they are often poorly filed, stored, and maintained. It is extremely difficult to establish an accurate and full inventory of urban buildings and structures by assembling building design plans in a piecemeal fashion. Although field surveys can be conducted to measure footprint and height of buildings, they are often labor intensive and time-consuming, and only limited urban area can be covered by the conventional ground surveys. Previously, Remote Sensing images and GIS have been employed to extract urban building information. Various remotely sensed data and classification methods have been used to derive the building coverage area (e.g., Gamba and Houshmand, 2000; Lhomme et al., 2009; Paparoditis et al., 1998; Shufelt, 1999; Thiele et al., 2007). In order to compute FAR, aerial stereo photogrammetry, InSAR data (Luckman and Grey, 2003; Thiele et al., 2007), and SRTM3 data (Liao et al., 2007) have been used to derive building height values. An average floor height value is often selected to estimate the total number of floors (Liao et al., 2007; Pan et al., 2008), and the gross floor area is calculated by multiplying the building coverage area to the floors' count. The complex building shape is often neglected in previous studies (Pan et al., 2008). With the remotely sensed image data, the accuracy of derived building height is severely affected by occlusions and shadows from man-made and natural objects in the urban areas (Baltsavias, 1999; Weidner and Forstner, 1995), or limited by the coarse resolution of image data (Liao et al., 2007). Han et al. (2005) proposed a Shaded Area Method, in which the size of building

shadows on high-resolution satellite images was used to estimate FAR through a regression model. The Shaded Area Method suffers from the drawbacks of low accuracy and time-consuming due to the requirement for manual extraction of building shadows. The Light Detection and Ranging (LiDAR) Remote Sensing technology represents a breakthrough for surveying and mapping buildings in urban environments. Surface elevation samples from airborne scanning are much more accurate, reliable and denser than those from the traditional photogrammetric techniques (Paolo Gamba and Houshmand, 2000, 2002; Priestnall et al., 2000; Stilla et al., 2003). The extraordinary capability of airborne LiDAR in gathering highly accurate and densely sampled surface elevation measurements over urban areas allows for an accurate delineation of the footprints of buildings (Ma, 2005; Yu et al., 2009b; Zhang et al., 2006) and reconstruction of the 3D building shapes (Forlani et al., 2006; Gamba and Houshmand, 2002; Rottensteiner, 2003).

This paper presents a new object-based method to automatically extract building objects and calculate various building density attributes, including BCR and FAR. Based on airborne LiDAR data, we derived, evaluated, and analyzed building density information for downtown Houston, Texas, USA. In the following sections, we first describe the case study area and the data sets used in the research. Then, we will present the algorithms and software implementations in detail for the object-based building density estimation method. Next, we will examine and contrast various building density attributes for different downtown districts of Houston. In the last section, we will summarize the research findings and draw some conclusions.

2. Case study area and data collection

Houston is the fourth largest city in the USA and is located in the coastal plain of the Gulf of Mexico. The downtown Houston is spatially bounded by Highway 45, Highway 10 and Highway 59 (Fig. 1a). A large cluster of high-rise buildings and skyscrapers have created a high-profile skyline in the downtown Houston. As a multi-functional center, the downtown Houston contains several distinct districts (Fig. 1a). These districts assume different functions such as retail, business, service, entertainments, or sports, and the types and shapes of buildings vary from district to district. The Skyline District contains the cluster of skyscrapers; the Theatre District is ranked second in terms of the number of theatre seats in the nation; the Historic District contains most of Houston's historic architecture and buildings; the Sports & Conventions district accommodates sports and convention venues, including Minute Maid Park (formerly Enron Field), the Toyota Centre, and the George Brown Convention Centre.

The LiDAR data were collected by an airborne system of TerraPoint LLC in 2001. According to the metadata, the Root Mean Square Error (RMSE) of LiDAR elevation measurements is estimated to be 11.6 cm and the average sampling density is 0.44 point per square meter. The LiDAR point measurements of the last return were provided by the Harris County Flood Control District (HCFCD) as x, y, z lists in an ASCII file. It should be noted, like many other early LiDAR surveys the LiDAR data used in our study only have the elevation (range) information, and the reflected intensity of the laser was not recorded. A Digital Surface Model (DSM) grid with a 1 m cell size was interpolated from the points by using the linear Triangulated Irregular Network (TIN) interpolation method. The DSM contains elevation information for all objects and ground features, including buildings and trees. By removing tree canopies and man-made structures, TerraPoint LLC has produced a bare-earth Digital Elevation Model (DEM) with its proprietary software system. Normalized DSM (nDSM), also known as Digital Height Model or Digital Object Model, is the difference between DSM and the bare-earth DEM

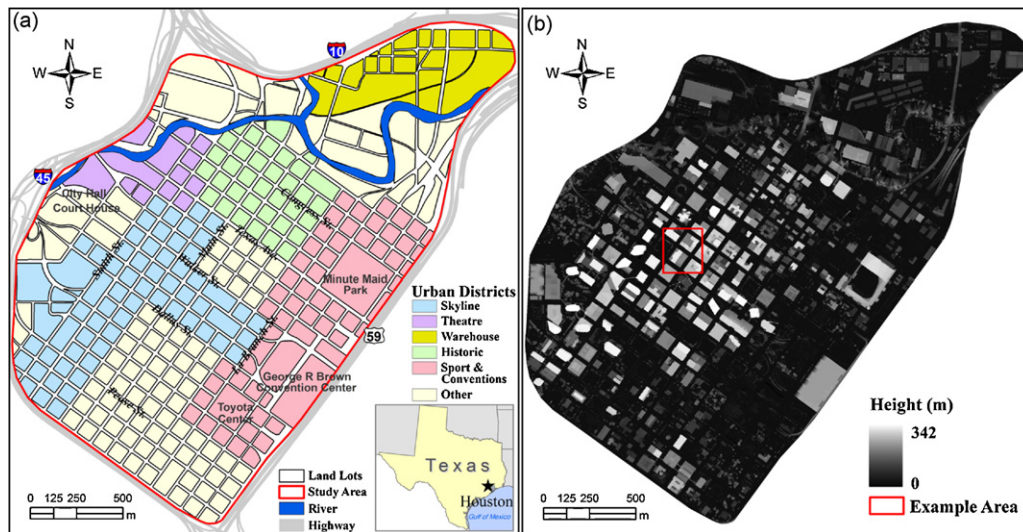


Fig. 1. Case study area and data. (a) Geographical location of downtown Houston; (b) nDSM from airborne LiDAR data.

(Haala and Brenner, 1999). The nDSM contains relative height information of man-made and natural objects rising above the ground. We created the nDSM of downtown Houston (Fig. 1b) by removing the bare-earth DEM value from the DSM grid.

The land lot data in vector format of downtown Houston was published by the City of Houston GIS (CoHGIS). We updated the land lot data with a reference to a recent 1 m resolution orthorectified color-infrared aerial image. The land lot map used in this research is shown in Fig. 1a.

The vegetation distribution information came from a detailed classification of urban landscape components by integrating airborne LiDAR and color near-infrared image data based on a new object-based two-stage method (Yu et al., 2009a,b, 2010). The color near-infrared aerial photograph used in this study was acquired on December 10, 2004. The photograph was orthorectified and distributed by the Texas Natural Resource Information System (TNRIS) as a DOQQ (Digital Orthophoto Quarter Quadrangle) image at 1 m spatial resolution. In the first stage of the method, the DOQQ images are used to segment the scene into image objects. Then, these objects are classified into three broad categories – impervious surface, vegetation, and water surface, based on their spectral and two-dimensional spatial attributes. In the second stage, the nDSM derived from airborne LiDAR data is introduced into analysis. Two indicators, relative height and roughness, of each vegetation object from the first stage are calculated, and the threshold values are determined to separate vegetation into lawns, shrubs/hedges, and trees. The overall classification accuracy of vegetation is analyzed and reported as high as 93.46% (Yu et al., 2010).

The data sets used in this research are all projected in UTM (Zone 15N) coordinate system with reference to WGS84 datum. And the vertical datum of the LiDAR data is the National Geodetic Vertical Datum of 1988 (NAVD 88).

3. Methods

3.1. Automated extraction of building objects

The nDSM from airborne LiDAR data represents the relative height information of man-made and natural objects rising above the ground, including buildings and vegetation canopies. Multi-spectral aerial photos and high-resolution satellite data are available, and the vegetation distribution has been classified and detected. In order to focus on the estimation of building density,

the vegetation coverage in downtown Houston is masked out from the original nDSM, and the remaining relative height values in nDSM correspond to the non-vegetated surface. The red rectangle bounded area in Fig. 1b is enlarged in Fig. 2 to illustrate the method. Fig. 2a is the original nDSM, and Fig. 2b is the masked nDSM after removing vegetation coverage.

After removing vegetation, a series of processing steps are applied to the nDSM to extract the objects and delineate the boundaries of buildings at a given height. Those processing steps include threshold-based segmentation, object identification, morphological operation, and boundary tracing

A threshold-based segmentation is adopted to transform the original nDSM to a segmented binary image by applying Eq. (1):

$$g(i, j) = \begin{cases} 1, & h(i, j) \geq H_0 \\ 0, & h(i, j) < H_0 \end{cases} \quad (1)$$

where $h(i, j)$ is the pixel relative height at row i and column j , H_0 is the threshold value, and $g(i, j)$ is the object code at pixel location (i, j) . An appropriate base building height (H_0) is selected as the threshold value to segment the nDSM and to extract the building objects. Different threshold values have been chosen to extract building objects in previous studies, e.g., 3 m in Ma (2005), and 4 m in Yu et al. (2009a,b). If the base building height H_0 is too high, many true buildings will be missed. On the other hand, if the selected base building height H_0 is too low, some small non-building objects like automobiles and street furniture will be mistakenly detected as building objects. We experimented with different threshold values between 3.0 m and 4.0 m, and observed that the extracted building objects are quite stable and do not change significantly with the variation of the threshold value in this range. Hence, we chose 3.5 m as the threshold value for our case study. Fig. 2c shows the segmentation result with this threshold value.

After the segmentation, the nDSM are recoded as a binary image to represent the portions of buildings rising above the threshold value (foreground) and other pixels (background). Those pixels with a relative height equal or larger than the threshold value 3.5 m are recoded as the foreground object pixels with a value of 1 (black in Fig. 2c), while the pixels with a relative height less than 3.5 m are recoded as non-building background pixels with a value of 0 (white in Fig. 2c).

The binary image consists of numerous spatially connected foreground regions, which represents building objects. These foreground regions in the segmented image need to be explicitly

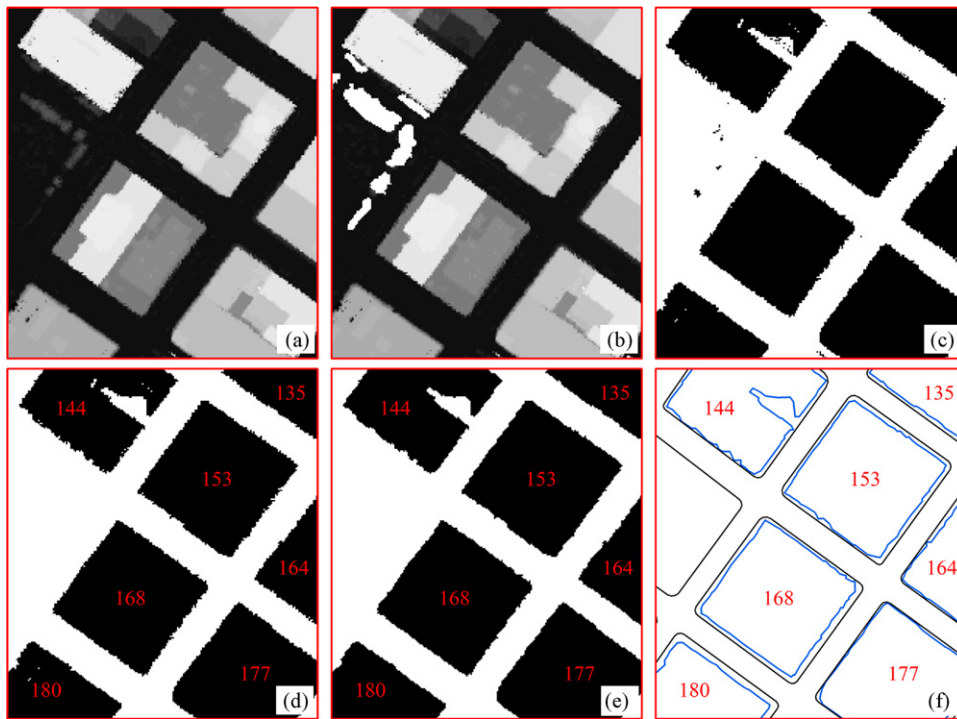


Fig. 2. Illustration of building object extraction process. (a) Original nDSM; (b) nDSM after removing vegetation canopy; (c) connected building pixels (black, recoded as 1); (d) buildings objects are identified and numbered; (e) morphological dilation and erosion; and (f) tracing and vectorizing edge pixels for delineating the boundaries of buildings.

identified and delimited as individual discrete objects for subsequent attribute computation. We used a recursive connected component identification and indexing algorithm (Liu and Jezek, 2004) to mark out the building objects based on the spatial 4-connectivity of the foreground pixels. First, the binary image is scanned in a row-wise manner, and a seed is set at the first foreground pixel, which is also treated as a single-cell building object. Next, this single-cell building object is expanded to include all building pixels immediately located in the 4-neighborhood of the current building pixel. During the expansion, the number of pixels in the current building object is accumulated. The expansion continues recursively until all contiguous building pixels are included. A threshold value of the object size is selected to remove small spurious objects, which might be induced by data noise. The derived building objects are indexed incrementally with a unique identification number (Fig. 2d).

Two types of morphological operations are applied to the building objects. Firstly, a filling operation (Sonka et al., 2007) is employed to fill the small internal holes whose size is smaller than a specified threshold value. Secondly, a closing operation (Sonka et al., 2007), which consists of a dilation operation immediately followed by an erosion operation, is used to effectively smooth the rough boundaries and close small gaps in the building objects (Fig. 2e). Both dilation operation and erosion operation are two types of basic morphological transformations for binary image. Dilation generally increases the sizes of objects, filling in holes and broken areas, and connecting areas that are separated by spaces smaller than the size of the structuring element. With binary images, dilation connects areas that are separated by spaces smaller than the structuring element and adds pixels to the perimeter of each image object. Erosion generally decreases the sizes of objects and removes small anomalies by subtracting objects with a radius smaller than the structuring element. With binary images, erosion completely removes objects smaller than the structuring element and removes perimeter pixels from larger image objects

(Sonka et al., 2007). The structure element adopted in this study is a 3×3 square.

After eliminating the spurious objects and smoothing object boundaries through morphology operations, a set of reliable and clean building objects are obtained. Then, the boundary of each object can be detected and traced. The boundary of an object is the set of pixels that are adjacent to at least one background pixel (Sonka et al., 2007). Technically, three types of boundary – inner, outer, and extended – can be derived (Sonka et al., 2007). The extended boundary is a better choice since it preserves the original shape of the object and provides the faithful common boundary acceptable by two adjacent objects (Feng and Pavlidis, 1975). We employ an extended boundary tracing algorithm (Liow, 1991) to detect edge pixels of the building objects. At last, a vector polygon is created by tracing the extended boundary pixels for each individual building object (Fig. 2f).

3.2. Associating individual buildings with corresponding land lots and urban districts

The location, size, and shape of land lots have been determined by using the data from the urban planning department of local government. To compute building density indicators, individual building objects derived from the object-based methods need to be associated with the corresponding land lots and urban districts.

Ideally, the boundaries of the buildings should be located entirely within the geographical borders of the land lots (e.g., No. 168 building object derived by object-based methods when using the threshold value of 3.5 m, see Fig. 3a). However, the extracted boundaries may slightly shift or extend out the land parcel due to the measurement or interpolation errors (e.g., No. 150 building object in Fig. 3b). In our analysis, the vectorized building boundaries are overlaid with the existing land lot layer. The topological relationships between these two layers are established. Then, the ratio of the part of the building object inside the land lot to the

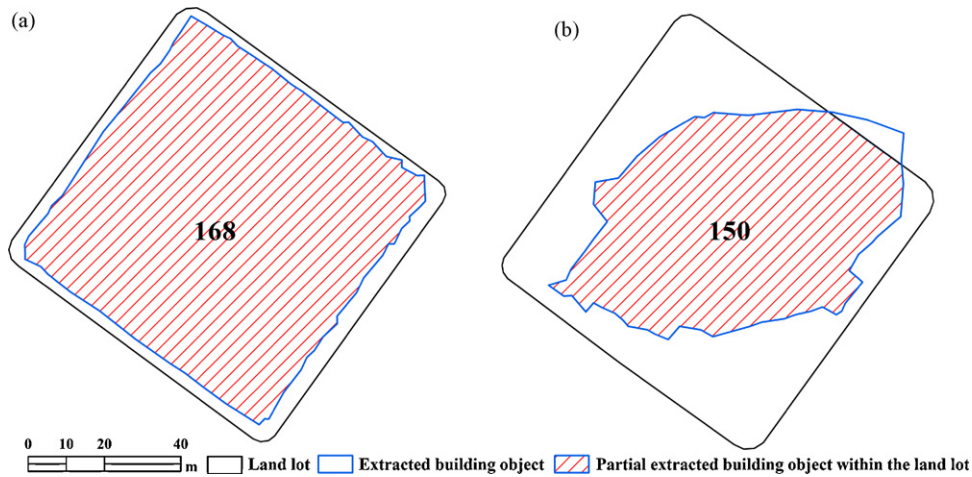


Fig. 3. Topological relationship between building object and land lot. (a) An extracted building object is completely within the land lot; (b) an extracted building object is partially intersecting with the land lot.

whole building object is calculated. If the ratio is larger than 0.9, namely, at least 90% of the building object is located in the geographical boundary of the corresponding land parcel, the building object is considered to be associated with that land lot. Otherwise, only the part of the building object that is located in the land lot is treated as the contribution area to the building density calculation.

3.3. Derivation of building density attributes

The recognition of building objects and their association with land lots and urban districts allow for the calculation of various building density attributes. The building density attributes derived in this analysis include three types: (1) geometric and volumetric attributes for individual buildings; (2) density attributes at the land lot scale; and (3) geometric, volumetric and density attributes at the urban district scale. These attributes can be used to characterize and analyze the physical form and structure of the urban landscape for urban environmental studies and land use management at different scales.

The geometric and volumetric attributes for individual buildings depict the geographical position and size of building footprints, and vertical dimensions of individual buildings. Those include the centroid coordinates (x_c, y_c) , perimeter (P) , and size (S) of building footprint, as well as the height (H) and volume (V) of building object. The numerical definitions of these attributes are listed in Table 1.

Building Coverage Ratio (BCR) and Floor Area Ratio (FAR) are the most commonly used indices for quantifying the building density at land lot scale. The BCR is defined as the ratio of the building

coverage area (i.e. the area of building footprint) to the size of land lot in Eq. (2).

$$BCR = \frac{S}{S_L} \tag{2}$$

where S is the building coverage area, and S_L is the area of land lot. Once the association between building footprints and land lots is determined, the BCR for each land lot can be computed using Eq. (2). Since the footprint represents the planimetric shape of a building, the BCR measures the building density in two-dimension (2D) space. The FAR is defined as the ratio of gross building floor area to the size of land lot (Eq. (3)).

$$FAR = \frac{\sum_{i=1}^t A_i}{S_L} \tag{3}$$

where A_i is the area of the i th floor, and t is the total number of floors. The value of FAR is determined not only by the planimetric shape of the building, but also by the vertical distribution of the floors in different height, it depicts the three-dimensional (3D) building density.

Fig. 4g shows a color-coded prismatic model for Building No. 168 in Fig. 2f. It is quite clear that this building has a complex vertical structure, and the size of floor area varies between floors. In order to obtain the accurate floor area estimate for each floor, a multi-threshold-based segmentation is applied to the nDSM. The footprint of the building object detected with the base height (H_0) represents the shape of the ground floor. Then, the threshold height values for the second and higher floors are determined by the base building height (H_0) , the number of floors (k) , and the average floor height (F) as in Eq. (4):

$$g_k(i, j) = \begin{cases} 1, & h(i, j) \geq (H_0 + (k - 1)F) \\ 0, & h(i, j) < (H_0 + (k - 1)F) \end{cases} \tag{4}$$

where $g_k(i, j)$ is the code number for the object representing the k th floor $(k = 1, 2, \dots, t)$. Different types of buildings will have different floor heights. For example, the average floor height of shopping malls and storage warehouses is much larger than that of residential buildings. In order to get an accurate estimate, we determined the average floor height value (F) for each urban district using a sample of building records. The segmented images for the k th floor will be treated and processed in a similar way to the building footprints described above. The objects at this level will be explicitly delimited to represent the k th floor of all buildings, and the area size of the objects will be calculated to represent the floor area for

Table 1
Definitions of geometric and volumetric attributes for individual buildings.

Attributes	Definition
Centroid point (x_c, y_c)	$x_c = \frac{1}{n} \sum_{i=1}^n x_i; y_c = \frac{1}{n} \sum_{i=1}^n y_i$
Perimeter (P)	$P = m_1 r + \sqrt{2} m_2 r$
Size (S)	$S = n r^2$
Height (H)	$H = \max\{h_i\}$
Volume (V)	$V = \sum_{i=1}^n h_i r^2$

where n is the number of cells consisting of building footprint object, (x_i, y_i) are the row and column coordinates of the i th cell of the object, m_1 is the number of boundary cell in horizontal or vertical orientation, m_2 is the number of boundary cell in diagonal step, r is the grid cell size, and h_i is the relative height value from LiDAR nDSM of i th cell in the footprint object.

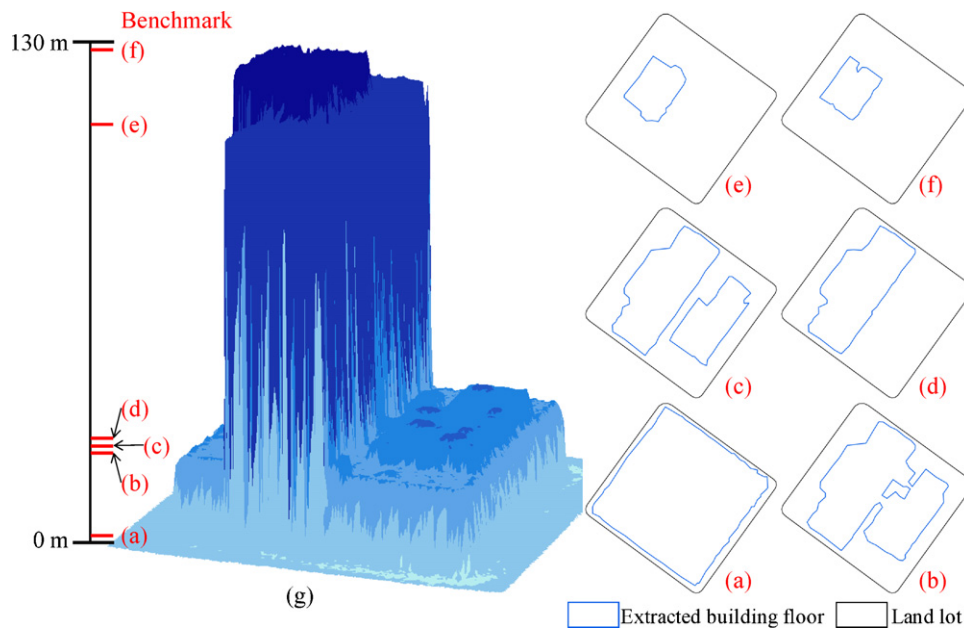


Fig. 4. The complex vertical shape and structure of building No. 168. Floor boundaries with multi-thresholds: (a) with threshold of 3.5 m; (b) with threshold of 21 m; (c) with threshold of 24.5 m; (d) with threshold of 28 m; (e) with threshold of 101.5 m; (f) with threshold of 108.5 m; (g) the color-coded prismatic model.

the k th floor. The sum of the floor areas for all floors within a land lot is used to compute the FAR value for the land lot.

Fig. 4 shows the boundaries of six floors derived by our object-based method for a complex building. The multi-threshold segmentation followed by the object-based building boundary extraction allows for the representation of the shape of each floor and hence more accurate estimate for the FAR value.

The geometric, volumetric and density attributes of buildings calculated at urban district scale include average building height (AV_H), average footprint size (AV_S), average building volume (AV_V), maximum building height (MAX_H), maximum building footprint size (MAX_S), maximum building volume (MAX_V), standard deviation of building height (SD_H), standard deviation of footprint size (SD_S), standard deviation of building volume (SD_V), number of buildings per hectare (BH), average nearest distance (AV_{ND}), average BCR (AV_{BCR}), average FAR (AV_{FAR}), overall BCR (OR_{FAR}), and overall FAR (OR_{FAR}). The numerical definitions of these attributes are shown in Table 2. A propagation-based distance transformation algorithm (Eggers, 1998) is adapted in this study to compute the distance between building objects. The propagation starts at the boundary of the buildings footprints. During propagation, the distance value will be recorded when meeting other building objects. The propagation ends when reaching the border of the whole research area. This set of attributes combine to give a comprehensive description of building density and landscape structure at urban functional or administrative district level.

3.4. Implementation and software tool

Our object-based building density estimation method has been implemented as an ArcGIS extension module with a Graphical User Interface. Algorithms for object extraction and building density attribute derivations are coded by using the computationally high performance C++ programming language, and the Graphic User Interface (GUI) is realized by using VB.Net and ArcObjects, which is a set of software components designed by ESRI Inc. specifically for developing ArcGIS applications and extensions.

The extension module is intended as a generic software tool for extracting urban building objects and deriving building density attributes based on the high-resolution data. The general data pro-

cessing scenario is shown in Fig. 5. In addition to the LiDAR nDSM grid, other input data include a mask grid of vegetation distribution, a vector data layer of land lot polygons, and a vector data layer of urban district polygons. Users can set the base building height and average floor height as threshold values for extracting urban building objects from LiDAR nDSM grid. Three sets of attributes can be produced as output products from this extension module. First, a set of geometric and volumetric attributes shown in Table 1 can be computed at individual building scale, and they are included as the feature attribute table associated with the extracted building object coverage (map). Second, the BCR and FAR can be computed at land lot scale and added into the feature attribute table of the land lot polygon coverage to create BCR and FAR maps. Third, a set of density attributes at urban district scale shown in Table 2 can be computed and added to the feature attribute table of the urban district polygon GIS data layer. Users can choose which set or which attributes in each set will be computed through the dialogue menu and dropdown lists of the GUI. The ArcGIS software has been widely used in urban planning and management communities. Seamlessly embedding urban building extraction and density attribute estimation functions into ArcGIS as its extension module allows users to take advantages of ArcGIS software package to manage the input data and visualize the building density calculation results. It also makes it easy to associate urban building density estimate results with other GIS data layers for further urban development policy analysis and decision making.

4. Results and discussions

We applied our object-based method and software tool to process the airborne LiDAR data for estimating urban building density indicators over downtown Houston at three different scales. With a base building height of 3.5 m as the threshold, the LiDAR nDSM grid is segmented into foreground and background pixels. Totally, 304 building objects are detected (Fig. 6). Then, the geometric and volumetric attributes are computed for these individual buildings.

By associating the extracted building objects with land lots, BCR and FAR indicators are computed and mapped at land lot scale (Figs. 7 and 8). Among 315 land lots/parcels in the downtown, 88 land lots remain open spaces and no buildings are detected. The

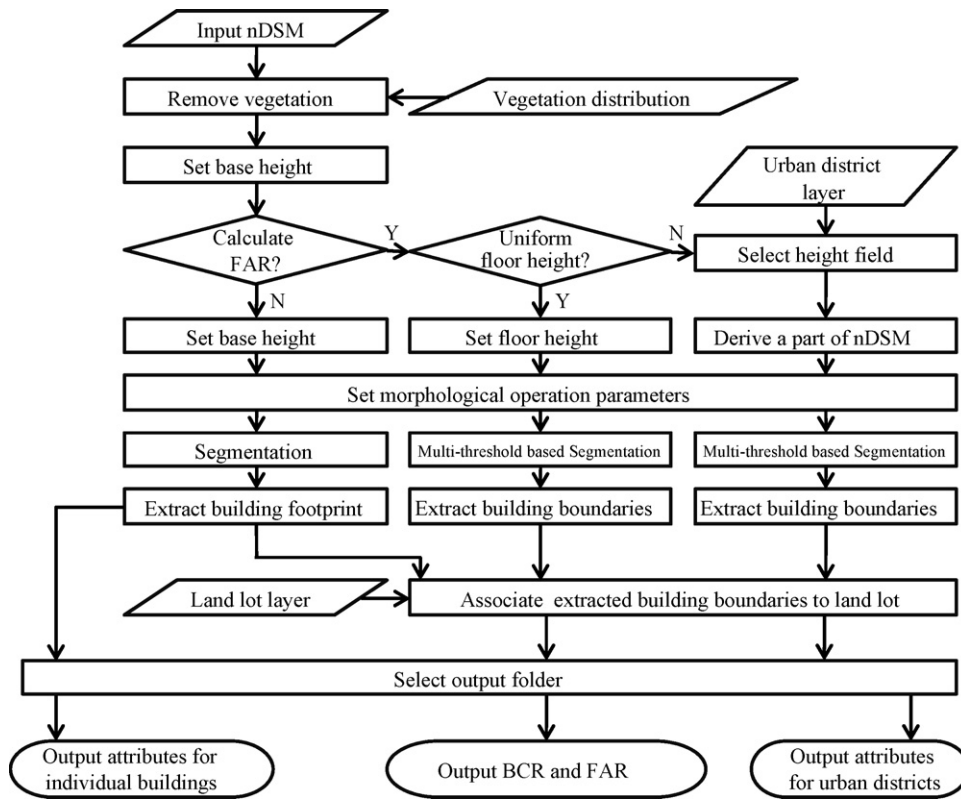


Fig. 5. Data processing flow chart for automated building density estimation.

remaining 227 lots are covered by buildings of varying density. The detection result is evaluated qualitatively through visual inspection and quantitatively through a sample of checking points. The visual inspection shows that the results closely match actual urban landscape components in position and shape. A major problem detected is that three buildings, the Toyota Center, Tundra Garage, and Hilton Americas-Houston, are misclassified as open spaces. This is because

the airborne LiDAR data were acquired three years earlier than the color near-infrared DOQQ image and these three structures did not exist at the time of the LiDAR survey. The detection accuracy is evaluated based on 500 check points selected with a random sampling scheme for the buildings and open spaces. The overall accuracy is as high as 96%. The results show that over 40% of land lots have a BCR value larger than 0.5, namely, more than half of the ground

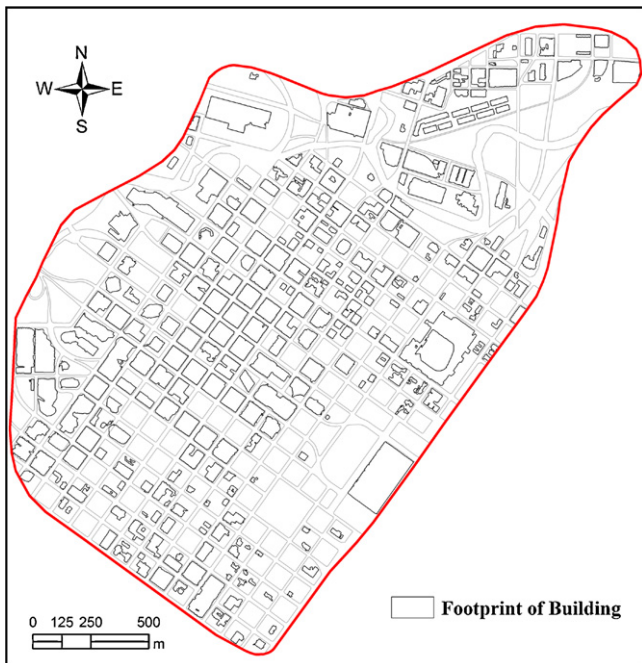


Fig. 6. Extracted building objects for downtown Houston.

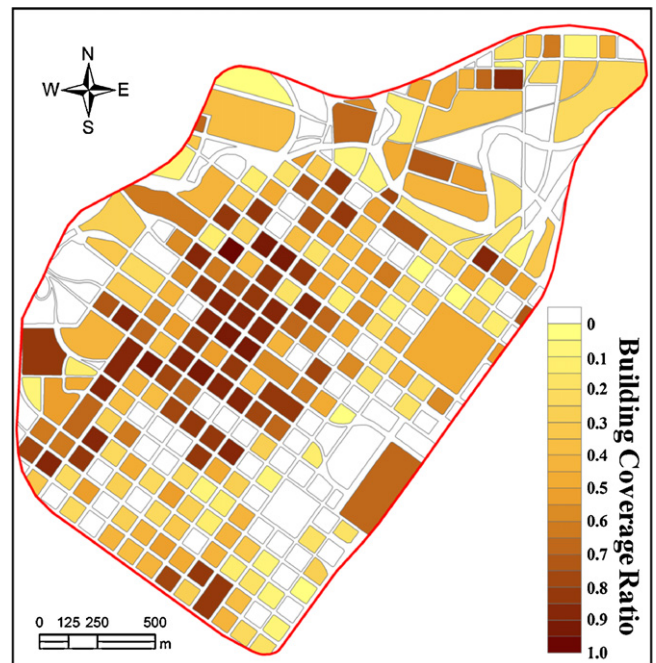


Fig. 7. Building Coverage Ratio map for downtown Houston.

Table 2
The definitions of density attributes at urban district scale.

Attributes	Definition
Average height (<i>AV.H</i>)	$AV.H = \frac{1}{b} \sum_{i=1}^b H_i$
Average size of footprint (<i>AV.S</i>)	$AV.S = \frac{1}{b} \sum_{i=1}^b S_i$
Average volume (<i>AV.V</i>)	$AV.V = \frac{1}{b} \sum_{i=1}^b V_i$
Maximum height (<i>MAX.H</i>)	$MAX.H = \max\{H_i\}$
Maximum size of footprint (<i>MAX.S</i>)	$MAX.S = \max\{S_i\}$
Maximum volume (<i>MAX.V</i>)	$MAX.V = \max\{V_i\}$
Standard deviation of height (<i>SD.H</i>)	$SD.H = \sqrt{\frac{\sum_{i=1}^b (H_i - AV.H)^2}{b}}$
Standard deviation of size (<i>SD.S</i>)	$SD.S = \sqrt{\frac{\sum_{i=1}^b (S_i - AV.S)^2}{b}}$
Standard deviation of volume (<i>SD.V</i>)	$SD.V = \sqrt{\frac{\sum_{i=1}^b (V_i - AV.V)^2}{b}}$
Number of buildings/hectare (<i>BH</i>)	$BH = \frac{b}{S_D \times 10,000^{-1}}$
Average nearest distance between buildings (<i>AV.ND</i>)	$AV.ND = \frac{1}{b} \sum_{i=1}^b ND_i$ $ND_i = \min\{D_{ij}\} (i \neq j)$
Average Building Coverage Ratio (<i>AV.BCR</i>)	$AV.BCR = \frac{1}{l} \sum_{i=1}^l BCR_i$
Average Floor Area Ratio (<i>AV.FAR</i>)	$AV.FAR = \frac{1}{l} \sum_{i=1}^l FAR_i$
Overall Building Coverage Ratio (<i>OR.BCR</i>)	$OR.BCR = \frac{\sum_{i=1}^b S_i}{S_D}$
Overall Floor Area Ratio (<i>OR.FAR</i>)	$OR.FAR = \frac{\sum_{j=1}^t \sum_{i=1}^{t_j} A_{ij}}{S_D}$

Where *b* is the total number of buildings in a single urban district, *H_i* is the height of the *i*th building in a single urban district, *S_i* is the footprint size of the *i*th building in a single urban district, *V_i* is the volume of the *i*th building in a single urban district, *S_D* is area of the urban district in m², *ND_i* is the nearest distance of the *i*th building to the other buildings in a same district, *D_{ij}* is the distance of the *i*th building to the *j*th building in a same urban district, *l* is the total number of land lots occupied by buildings, *BCR_i* is the Building Coverage Ratio of the *i*th land lot occupied by buildings in a single urban district, *FAR_i* is the Floor Area Ratio of the *i*th land lot occupied by buildings in a single urban district, *t_j* is the total number of floors of *j*th building in a single urban district, and *A_{ij}* is the area of the *i*th floor in the *j*th building in a single urban district.

Table 3
Floor heights adopted for different urban districts.

Urban districts	Floor height (m)
Skyline	3.5
Theatre	4.0
Historic	3.0
Warehouse	5.0
Sports & Conventions	4.0
Other	3.5

space for these lots are occupied by building structures (Fig. 7). The most intensively developed land lot has a BCR value as high as 0.96, namely, almost the entire ground surface is covered by building structures and not much open space exists for the lot.

The FAR is estimated in two ways. First, a uniform floor height (*F*) of 3.5 m is used in Eq. (4) to derive the floor areas for all land lots in the downtown, and the spatial distribution of the FAR value is shown Fig. 8a. There are 35 land lots where the FAR value is larger than 10.0. As expected, land lots in the Skyline District have high FAR values, and the average FAR value for the Skyline District reaches 11.9 if only take the land parcels with buildings into account. In other words, buildings in the Skyline District have about 12 floors on average. Second, different floor height values are chosen for six different urban districts (Table 3) in consideration of the fact that the type of building varies from district to district. Buildings in the Theatre, Warehouse, and Sports & Conventions districts tend to have a higher floor height, while buildings in historic district have a smaller floor height. Fig. 8b shows the FAR distribution calculated with varied floor height values for different urban districts. Although the spatial pattern remains the same, the magnitude of FAR values is considerably reduced for the land lots in the Warehouse District and Sports & Conventions District due to the adoption of a higher floor height.

We have made an assessment on the accuracy of our calculation results. Actual heights for 10 buildings are acquired from the Emporis.com, a database of commercial real estate information and construction (<http://www.emporis.com/en/wm/ci/bu/?id=101031>), as ground truth. By comparing our computational results from the LiDAR data to the EMPORIS records, the overall accuracy for building height is better than 98%. In addition, the reference data for building footprints are developed by manually tracing building boundaries from 1 m resolution orthorectified color-infrared aerial photographs. Our comparison shows that the building objects numerically derived from the LiDAR data closely match the manually traced building footprints in position and shape. The overall

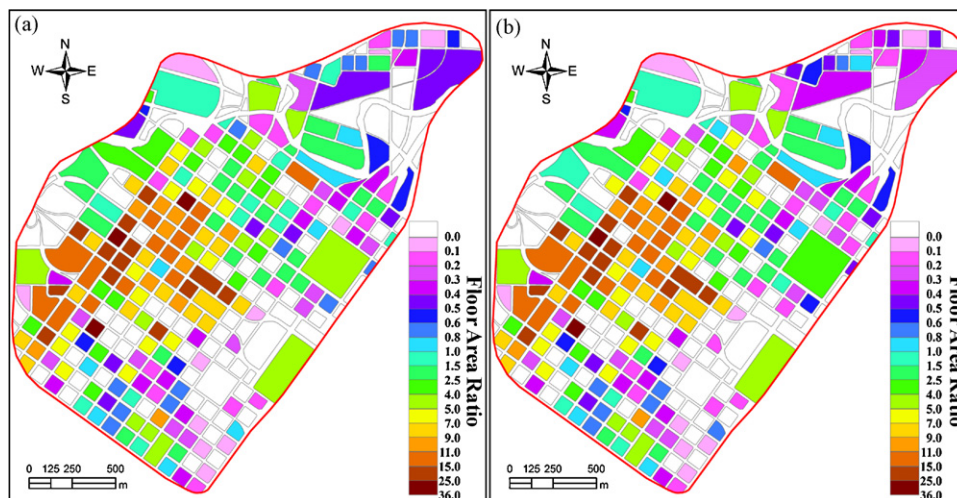


Fig. 8. Floor Area Ratio maps of downtown Houston. (a) With a uniform floor height of 3.5 m; (b) with varied floor heights for different districts.

Table 4
Building density attributes calculated for different urban districts.

Districts	Area (m ²)	Number of buildings	BH	AV.H (m)	AV.S (m ²)	AV.V (m ³)	MAX.H (m)	MAX.S (m ²)	MAX.V (m ³)
Skyline	792,646	64	0.81	118.47	5370	338,662	341.80	27,374	1,005,060
Theatre	227,718	11	0.48	40.90	5844	151,416	112.54	20,116	328,461
Historic	366,535	44	1.20	34.40	2687	66,947	109.27	11,349	658,929
Warehouse	394,785	35	0.89	11.52	2357	17,546	29.72	10,304	88,007
Sports & Conventions	828,131	50	0.60	17.11	2914	64,746	75.55	42,118	1,361,790
Other	1,622,586	100	0.62	27.24	2995	64,031	121.27	24,859	494,524
Districts	SD.H (m)	SD.S (m ²)	SD.V (m ³)	AV.ND (m)	AV.BCR	AV.FAR	OR.BCR	OR.FAR	
Skyline	83.64	3899	247,929	17.69	0.65	11.93	0.43	7.69	
Theatre	29.19	5802	119,800	37.29	0.42	2.98	0.28	1.69	
Historic	22.61	2431	108,211	17.22	0.54	3.80	0.32	2.54	
Warehouse	5.59	2314	19,580	16.06	0.36	0.35	0.21	0.21	
Sports & Conventions	13.91	7669	252,404	34.04	0.32	0.82	0.18	0.69	
Other	26.53	3719	95,051	22.98	0.41	2.47	0.19	1.04	

accuracy for building object (footprint) size is estimated to be better than 90%.

Various building density indicators have been derived for six districts of downtown Houston (Table 4). These indicators combine to provide a comprehensive and quantitative view on the morphology and spatial structure of urban landscape in downtown Houston.

Downtown Houston represents one of the most complex urban landscapes crowded with structures of different natures and heights. A large number of high-rise buildings and skyscrapers are concentrated in the Skyline District. The buildings are densely distributed, and the average nearest distance between buildings is only 17.7 m. This district best reflects the vertical expansion of the urban landscape and is almost three times as high as the second highest district – the Theatre District. The tallest building is over 300 m above the ground. The average height of buildings in the Skyline District is as high as 118 m, and the overall FAR concerning varied floor heights for different districts is 7.7. Due to the vertical dimension and relatively large footprint, most buildings in the Skyline District also have a large volume. The average volume of buildings in the Skyline District is greatly larger than in other districts. This district represents the highest man-made relief in the downtown. It also should be noted that the building height and volume vary drastically from building to building in the Skyline District, which are indicated by the large standard deviation of building height and volume. Therefore, the dense cluster of buildings also forms “rugged” urban morphology in the Skyline District.

Buildings in the Theatre District and the Sports & Conventions District are relatively sparsely distributed, and more open space, parking lots and lawns are available to accommodate the functionalities of entertainment, sports and convention facilities. These two districts have a low building density, 0.48 and 0.60 buildings per hectare respectively. The spacing between buildings is relatively large, and the average nearest distance between buildings in these two districts is more than two times as large as in other districts. Some bulky and giant buildings are scattered in these two districts. The Theater District is ranked second in terms of the number of theater seats in the nation, only behind New York City. A number of famous theaters, including the Wortham Center (opera & ballet), the Alley Theater, the Hobby Center (musical, concerts, events), Jones Hall (symphony), Verizon Wireless Theater (concerts and events), are located in this district. On average, the buildings in the Theatre District have the largest base floor area (footprint) among different districts. Although buildings in the Sport & Conventions District are low in vertical dimension in general, the horizontal dimension (indicated by the footprint size) and the volume of some buildings are enormous. In fact, the largest buildings in terms of footprint size and volume are located in the Sports & Conventions District rather than in the Skyline District. The

Minute Maid Park stadium has a volume of 1,361,790 m³, while the George R Brown Convention Center has a volume of 1,205,690 m³. In the Warehouse District, buildings are dense, and the average nearest distance between buildings is only 16 m. Most of buildings have a low and similar height. The overall BCR and FAR have almost same value of 0.21 in this district, which demonstrates this district has a relatively homogenous surface and is dominated by horizontal “low-altitude” extension of urban development. The Historic District contains most of Houston’s historic architecture and buildings. This district has the highest building density in terms of the number of buildings per hectare. The overall BCR is 0.3, and the average nearest distance between buildings is 17.2 m in this district. Nevertheless, building height and size are considerably smaller than those in the Skyline District and the Theatre District.

5. Conclusions

The scientific knowledge of urban building density information is fundamentally important for intelligent management and planning of the urban environment. The airborne LiDAR technology provides the extraordinary capability in gathering highly accurate and densely sampled surface elevation measurements over urban areas. Through a case study in downtown Houston, we have demonstrated that unprecedented detail level of accurate building density information can be automatically and efficiently derived from airborne LiDAR data. We developed an effective object-based method and software tool that is capable of extracting building objects and computing various building density indicators at three different scales. First, a set of geometric and volumetric attributes are computed at individual building scale to describe the size and shape of buildings. Second, by associating with land lots through topological operation, two most widely used building density indicator, BCR and FAR, are computed and mapped at land lot scale. Third, a suite of density attributes are computed at urban district scale to provide quantitative description of the 3D spatial structure of urban landscape. The object-based methods and associated algorithms have been implemented as an ArcGIS extension module with a graphical users interface. We believe this software tool would be useful for the urban planning and management community to characterize and quantify urban building density based on the newly available LiDAR data.

Buildings and man-made structures are densely populated in downtown Houston, forming a complex urban landscape. Since different districts accommodate distinct urban economic, social and cultural functions, the building size, height, volume, density, morphological heterogeneity and vertical roughness vary from district to district. The BCR map shows the planimetric and horizontal density of buildings, while the FAR map shows the 3D density of

building. The Skyline District best embodies the vertical extension of urban growth with extremely high land use intensity. This district represents highest and most rugged relief of the artificial urban terrain. In contrast, the Warehouse District is dominated with low-altitude horizontal extension of urban growth with a relatively low vertical roughness. Large and bulky buildings are scattered in Theatre District and Sports & Convention District, where buildings are spaced with relative large open spaces. As demonstrated, attributes that we derived at three different scales give a comprehensive and quantitative description on the building density, urban physical form, and morphology of urban space from different angles. We believe that the quantitative building density information would be useful for studying urban environment and managing urban land development and growth.

Acknowledgments

The authors are grateful to the anonymous reviewers for their constructive comments and suggestions. This study is supported by the Fundamental Research Funds for the Central Universities of China.

References

- Adolphe, L., 2001. A simplified model of urban morphology: application to an analysis of the environmental performance of cities. *Environ. Plan. B-Plan. Des.* 28 (2), 183–200.
- Arnott, R.J., MacKinnon, J.G., 1977. Measuring the costs of height restrictions with a general equilibrium model. *Reg. Sci. Urban Econ.* 7 (4), 359–375.
- Baltsavas, E.P., 1999. A comparison between photogrammetry and laser scanning. *ISPRS-J. Photogram. Remote Sens.* 54 (2–3), 83–94.
- Bertaud, A., Brueckner, J.K., 2005. Analyzing building-height restrictions: predicted impacts and welfare costs. *Reg. Sci. Urban Econ.* 35 (2), 109–125.
- Chau, K.W., Wong, S.K., Yau, Y., Yeung, A.K.C., 2007. Determining optimal building height. *Urban Stud.* 44 (3), 591–607.
- Cionco, R.M., Ellefsen, R., 1998. High resolution urban morphology data for urban wind flow modeling. *Atmos. Environ.* 32 (1), 7–17.
- Cui, Z.D., Tang, Y.Q., Yan, X.X., Yan, C.L., Wang, H.M., Wang, J.X., 2010. Evaluation of the geology-environmental capacity of buildings based on the ANFIS model of the floor area ratio. *Bull. Eng. Geol. Environ.* 69 (1), 111–118.
- Eggers, H., 1998. Two fast euclidean distance transformations in Z^2 based on sufficient propagation. *Comput. Vis. Image Underst.* 69 (1), 106–116.
- Feng, H.Y.F., Pavlidis, T., 1975. The generation of polygonal outlines of objects from gray level pictures. *IEEE Trans. Circuit Syst.* 22 (5), 427–439.
- Forlani, G., Nardinocchi, C., Scaioni, M., Zingaretti, P., 2006. Complete classification of raw LIDAR data and 3D reconstruction of buildings. *Pattern Anal. Appl.* 8 (4), 357–374.
- Frenkel, A., 2007. Spatial distribution of high-rise buildings within urban areas: the case of the Tel-Aviv metropolitan region. *Urban Stud.* 44 (10), 1973–1996.
- Fu, Y., Somerville, C.T., 2001. Site density restrictions: measurement and empirical analysis. *J. Urban Econ.* 49 (2), 404–423.
- Gamba, P., Houshmand, B., 2000. Digital surface models and building extraction: a comparison of IFSAR and LIDAR data. *IEEE Trans. Geosci. Remote Sens.* 38 (4), 1959–1968.
- Gamba, P., Houshmand, B., 2002. Joint analysis of SAR, LIDAR and aerial imagery for simultaneous extraction of land cover, DTM and 3D shape of buildings. *Int. J. Remote Sens.* 23 (20), 4439–4450.
- Gao, X.L., Asami, Y., Katsumata, W., 2006. Evaluating land-use restrictions concerning the floor area ratio of lots. *Environ. Plan. C-Gov. Policy* 24 (4), 515–532.
- Greer, S.A., 1980. *Urban Renewal and American Cities*. The Bobbs-Merrill Co. Inc., New York.
- Haala, N., Brenner, C., 1999. Extraction of buildings and trees in urban environments. *ISPRS-J. Photogram. Remote Sens.* 54 (2–3), 130–137.
- Han, X., Xu, J., Fu, X., 2005. A study on estimating urban FAR based on high-resolution satellite images. *Remote Sens. Inf.* (2), 24–28 (in Chinese with English abstract).
- Hartshorn, T.A., 1992. *Interpreting the City: An Urban Geography*, 2nd ed. Wiley, New York.
- Joshi, K.K., Kono, T., 2009. Optimization of floor area ratio regulation in a growing city. *Reg. Sci. Urban Econ.* 39 (4), 502–511.
- Kono, T., Kaneko, T., Morisugi, H., 2008. Necessity of minimum floor area ratio regulation: a second-best policy. *Ann. Reg. Sci.*, doi:10.1007/s00168-008-0269-0.
- Kubota, T., Miura, M., Tominaga, Y., Mochida, A., 2008. Wind tunnel tests on the relationship between building density and pedestrian-level wind velocity: development of guidelines for realizing acceptable wind environment in residential neighborhoods. *Build. Environ.* 43 (10), 1699–1708.
- Lam, J.C., 2000. Shading effects due to nearby buildings and energy implications. *Energy Conv. Manag.* 41 (7), 647–659.
- Lhomme, S., He, D.-C., Weber, C., Morin, D., 2009. A new approach to building identification from very-high-spatial-resolution images. *Int. J. Remote Sens.* 30 (5), 1341–1354.
- Liao, B., Han, X., Xu, J., 2007. Estimating floor area ratio based on SRTM3 and land use data. In: Paper Presented at the Geoinformatics 2007: Geospatial Information Science (Proc. SPIE), Nanjing.
- Liow, Y.-T., 1991. A contour tracing algorithm that preserves common boundaries between regions. *CVGIP: Image Underst.* 53 (3), 313–321.
- Liu, H., Jezek, K.C., 2004. Automated extraction of coastline from satellite imagery by integrating Canny edge detection and locally adaptive thresholding methods. *Int. J. Remote Sens.* 25 (5), 937–958.
- Luckman, A., Grey, W., 2003. Urban building height variance from multibaseline ERS coherence. *IEEE Trans. Geosci. Remote Sens.* 41 (9), 2022–2025.
- Ma, R.J., 2005. DEM generation and building detection from Lidar data. *Photogramm. Eng. Remote Sens.* 71 (7), 847–854.
- Miguet, F., Groleau, D., 2002. A daylight simulation tool for urban and architectural spaces – application to transmitted direct and diffuse light through glazing. *Build. Environ.* 37 (8–9), 833–843.
- Mills, G., 1997. Building density and interior building temperatures: a physical modeling experiment. *Phys. Geogr.* 18 (3), 195–214.
- Narayan, R.K., 1996. *Urban Redevelopment: A Study of High-rise Buildings*. Concept Pub. Co., New Delhi.
- Oke, T.R., 1988. Street design and urban canopy layer climate. *Energy Build.* 11 (2), 103–113.
- Pan, X.Z., Zhao, Q.G., Chen, J., Liang, Y., Sun, B., 2008. Analyzing the variation of building density using high spatial resolution satellite images: the example of Shanghai City. *Sensors* 8 (4), 2541–2550.
- Papadimitris, N., Cord, M., Jordan, M., Cocqueruz, J.P., 1998. Building detection and reconstruction from mid- and high-resolution aerial imagery. *Comput. Vis. Image Underst.* 72 (2), 122–142.
- Priestnall, G., Jaafar, J., Duncan, A., 2000. Extracting urban features from LiDAR digital surface models. *Comput. Environ. Urban Syst.* 24 (2), 65–78.
- Robinson, D., 2006. Urban morphology and indicators of radiation availability. *Sol. Energy* 80 (12), 1643–1648.
- Rottensteiner, F., 2003. Automatic generation of high-quality building models from Lidar data. *IEEE Comput. Graph. Appl.* 23 (6), 42–50.
- Shufelt, J.A., 1999. Performance evaluation and analysis of monocular building extraction from aerial imagery. *IEEE Trans. Pattern Anal. Mach. Intell.* 21 (4), 311–326.
- Sonka, M., Hlavac, V., Boyle, R., 2007. *Image Processing, Analysis, and Machine Vision*, 3rd ed. Thomson, Toronto.
- Stilla, U., Soergel, U., Thoennessen, U., 2003. Potential and limits of InSAR data for building reconstruction in built-up areas. *ISPRS-J. Photogram. Remote Sens.* 58 (1–2), 113–123.
- Streutker, D.R., 2003. Satellite-measured growth of the urban heat island of Houston. *Texas Remote Sens. Environ.* 85 (3), 282–289.
- Swaid, H., 1993. The role of radiative-convective interaction in creating the microclimate of urban street canyons. *Bound.-Layer Meteorol.* 64 (3), 231–259.
- Theodoridis, G., Moussiopoulos, N., 2000. Influence of building density and roof shape on the wind and dispersion characteristics in an urban area: a numerical study. *Environ. Monit. Assess.* 65 (1–2), 407–415.
- Thiele, A., Cadario, E., Schulz, K., Thoennessen, U., Soergel, U., 2007. Building recognition from multi-aspect high-resolution InSAR data in urban areas. *IEEE Trans. Geosci. Remote Sens.* 45 (11), 3583–3593.
- Wang, M.S., Chien, H.T., 1999. Environmental behaviour analysis of high-rise building areas in Taiwan. *Build. Environ.* 34 (1), 85–93.
- Weidner, U., Forstner, W., 1995. Towards automatic building extraction from high-resolution digital elevation models. *ISPRS-J. Photogram. Remote Sens.* 50 (4), 38–49.
- Weiss, M.A., 1992. Skyscraper zoning: New York's pioneering role. *J. Am. Plan. Assoc.* 58 (2), 201–212.
- Wong, K.M.G., 2004. Vertical cities as a solution for land scarcity: the tallest public housing development in Singapore. *Urban Des. Int.* 9 (1), 17–30.
- Yu, B., Liu, H., Wu, J., 2010. A method for urban vegetation classification using airborne LiDAR data and high resolution remote sensing images. *J. Image Graph.* 15 (5), 782–789 (in Chinese with English abstract).
- Yu, B., Liu, H., Wu, J., Lin, W.-M., 2009a. Investigating impacts of urban morphology on spatio-temporal variations of solar radiation with airborne LiDAR data and a solar flux model: a case study of downtown Houston. *Int. J. Remote Sens.* 30 (17), 4359–4385.
- Yu, B., Liu, H., Zhang, L., Wu, J., 2009b. An object-based two-stage method for a detailed classification of urban landscape components by integrating airborne LiDAR and color infrared image data: a case study of downtown Houston. In: Paper presented at the 2009 Joint Urban Remote Sensing Event, Shanghai.
- Zhang, K., Yan, J., Chen, S.-C., 2006. Automatic construction of building footprints from airborne LIDAR data. *IEEE Trans. Geosci. Remote Sens.* 44 (9), 2523–2533.